Zhihong Li, Francesco Chiavaioli, **"In-fiber comb-like linear polarizer with leaky mode resonances"**, OPTICS AND LASER TECHNOLOGY, vol. 133, 2021, https://dx.doi.org/10.1016/j.optlastec.2020.106518

In-fiber comb-like linear polarizer with leaky mode resonances

Zhihong Li[a,b,*], Francesco Chiavaioli[c,*]

[a] *College of Electrical and Electronic Engineering, Wenzhou University, Wenzhou 325035, China*
[b] *National-Local Joint Engineering Laboratory for Digitalize Electrical Design Technology, Wenzhou University, Wenzhou 325035, China*
[c] *Institute of Applied Physics "Nello Carrara" (IFAC), National Research Council of Italy (CNR), Sesto Fiorentino 50019, Italy*

Abstract

Leaky mode resonance (L^{e}MR) has been proven as a promising high-performance and effective technology for fiber-optic devices. Here, we propose and theoretically demonstrate an in-fiber comb-like linear polarizer based on enhanced L^{e}MR (eL^{e}MR) in tilted fiber grating (TFG) with indium tin oxide (ITO) nanocoating. The ITO nanocoating induces the guidance of TE-polarized leaky modes, and hence greatly enhances the mode coupling with the core guided mode, which leads to the excitation of dense comb-like TE eL^{e}MRs. By optimizing the ITO thickness and grating length, the results show that the eL^{e}MRs can be designed to realize a novel in-fiber comb-like linear polarizer with remarkable polarization extinction ratio (PER) up to 57 dB and ultra-narrow bandwidth (full width at half maximum, FWHM) smaller than 0.5 nm, together with wavelength separation between adjacent bands equal to 3.1 nm, in a broad wavelength range. Moreover, the operating wavelength of the polarizer can be further tuned by tailoring the grating parameters, like the period and tilt angle of the TFG. The designed polarizer will cover a wide range of applications including multi-wavelength fiber lasers, dense wavelength-division-multiplexed (DWDM) systems, optical spectrometers, and fiber-optic sensing systems.

Keywords: In-fiber linear polarizer, Leaky mode resonances, Tilted fiber grating, Metal oxide materials

1. Introduction

Optical polarizers are of great importance for discrimination between orthogonal linear polarization states of electromagnetic waves. Compared with conventional polarizers, inline optical fiber polarizers feature several advantages such as small size, low insertion loss, good stability and perfect compatibility with optical telecommuni-

*Corresponding author
Email addresses: zhihong@wzu.edu.cn (Zhihong Li), f.chiavaioli@ifac.cnr.it (Francesco Chiavaioli)

cation systems [1]. One of the most widespread techniques for realization of inline fiber polarizer is to fabricate a hybrid structure that consists of etched or polished optical fiber and nanocoatings embedded into fiber surface [2]. In this structure, the polarizing mechanism is based on the polarization-dependent interaction between the evanescent field of guided modes and the nanocoatings [3]. Many kinds of thin-films have been used to achieve fiber polarizers, such as metal film [4, 5], graphene [6, 7], carbon nanotube [8], polymer [9, 10], liquid crystal [11], etc. Among them, the metal film based fiber polarizers that depend on the TM-polarized surface plasmon resonance (SPR) are the most preferred ones for linear polarization selectivity. However, they have some disadvantages. The SPR can be excited only when the phase matching condition (PMC) is satisfied, which means that there is a very limited tunability for the polarization selectivity. In addition, the SPR generally exists at the wavelength that is far away from the telecommunication band at lowest loss ($1530\,nm \sim 1565\,nm$). It is worth pointing out that the SPR can be also generated by some other materials (not only noble metals) like indium tin oxide (ITO), but at wavelengths larger than 2 µm (middle infrared) where the optoelectronic equipment is more expensive and less compatible with other standard instrumentations [12].

Graphene, an ultra-thin two-dimensional material with gapless band dispersion, has become a promising alternative material for realization of optical polarizers with excellent tunable features [13–15]. Depending on its dynamic conductivity, graphene can be tuned to support the propagation of TE or TM light in a wide frequency range and hence a broadband TE-/TM-pass polarizer can be realized [6, 7, 16]. For instance, a graphene based side-polished fiber polarizer has been reported, demonstrating a polarization extinction ratio (PER) up to $27\,dB$ at $1500\,nm$ [7]. Of this particular configuration, the light-graphene interaction is enhanced by integrating additional nanocoatings like polyvinyl butyral (PVB) and polymethyl methacrylate (PMMA) to further optimize the polarizing performance [9, 10].

Other kinds of fiber polarizers have also been reported, such as the configurations based on microstructured optical fibers (MOFs) and fiber gratings [17, 18]. The MOFs have specially designed air holes that can selectively be filled with several materials to tune the propagation properties of guided light. For example, the infiltration of materials like nano film and nano particles/wires into air holes induces a strong polarization-dependent absorbance of guided light, which leads to a tunable TE-/TM-pass polarizer [19, 20]. The disadvantage of the MOF polarizer lies in the fabrication process that requires very precise and expensive equipment.

Fiber-optic gratings realized by laser irradia-

tion, micro-bends or twisting have also been proposed as inline polarizer [21, 22]. In particular, fiber-optic gratings inscribed by ultraviolet laser irradiation provides a stable platform for in-fiber polarizers without breaking the fiber structure or modifying its geometry. Among them, tilted fiber gratings (TFGs) are characterized by a highly polarization-dependent mode coupling behavior due to its asymmetric grating structure and index modulation. [23, 24]. Depending on the mechanism of mode coupling, the TFGs can be simply classified as tilted fiber Bragg gratings (TFBGs), 45° TFGs and excessively TFGs (Ex-TFGs). TFBGs possess dense counter-propagating cladding mode resonances in the transmission spectrum that have been used to different applications, both in sensing and in telecommunication. However, in the latter case, the performances in terms of polarization extinction ratio (PER) cannot be considered satisfactory (due to very small difference between TE- and TM-polarized resonances in bare TFBGs), thus preventing them to be effectively used alone as linear polarizers. When the tilt angle approaches the Brewster's angle, the TFG is known as 45° TFG that allows coupling the TE-polarized core mode into radiation modes, while the residual TM light propagates along the fiber core with a minimal loss, leading to a wide polarization-dependent resonance band in the transmission spectrum that follows the Gaussian distribution [25]. In this sense, the 45° TFG represents an ideal in-fiber polarizer with some advantages, such as high PER, broadband response range, low insertion loss and wavelength tunability [26–29]. On the other hand, high performances can be attained at 45° tilt angle only (other tilt angles result in much lower PER), a not easy condition for the grating inscription compared to standard tilt angles ($6° \sim 30°$ in general). Furthermore, additional wavelength selection devices like FBGs are necessary to select the desired wavelength since the 45° TFG is characterized by a wide spectrum, and hence does not possess the inherent capability of wavelength selection. In addition, the use of adjacent wavelength components should be taken into account when the 45° TFG with a wide spectral range without discontinuities is employed in wavelength-routing devices or multi-wavelengths sources. Finally, when the tilt angle increases further and becomes greater than 80°, the TFGs are named excessively TFGs presenting a transmission spectrum similar to long period fiber gratings, except for the generation of additional polarization-dependent resonances corresponding to the coupling with higher-order modes that degenerate into two orthogonal polarization states (TE and TM), showing the typical dual-peak feature on the spectrum [30, 31]. Clearly, Ex-TFGs exploit also peculiar polarization property even if they are largely used in sensing due to wider resonances, which do not make them an ideal platform for in-fiber polarizers.

More recently, a new kind of electromagnetic resonance, i.e. enhanced leaky mode resonance (eL^{e}MR) with improved response to surrounding medium changes, was reported in the TFG with different nanocoatings including graphene, metal film and metal oxide [32–34]. It was found that the eL^{e}MR shows strong polarization dependence on the dielectric properties of the thin film. For instance, both TE- and TM-polarized leaky modes can be excited to generate dense comb-like eL^{e}MRs by metal film while only the first few TE-polarized eL^{e}MRs are attained with graphene. In this sense, the eL^{e}MRs are preferable for either comb-like filters with no polarization dependence in a wide wavelength range (for the case with metal film) or linear polarizer at specific wavelengths (for the case with graphene). Similar with the metal film, the metal oxide with high refractive index can also excite dense comb-like eL^{e}MRs but with strong polarization dependence, which makes it suitable for in-fiber comb-like linear polarizer. However, there are two critical issues that are not yet taken into account: one is the excitation of strong dense comb-like polarization-dependent eL^{e}MRs in air environment at which optical devices usually operate, and the other is the optimization of polarizing performance indicated in terms of PER and bandwidth.

In this work, we propose and investigate in depth an in-fiber comb-like linear polarizer based on a TFG with metal oxide nanocoating (indium tin oxide, ITO). The ITO film with optimized thickness leads to the guidance of TE-polarized leaky modes, indicated by a greatly decreased loss. This reduction allows strong coupling from the forward propagating core mode into the backward TE leaky modes, leading to strong dense comb-like eL^{e}MRs with ultra-narrow bandwidth in a broad wavelength range. Therefore, a high contrast between the TE- and TM-polarized resonances is obtained, which can be used to realize a comb-like linear polarizer. The polarizer with the PER up to $57\,dB$ and the full width at half maximum (FWHM) less than $0.5\,nm$, together with wavelength separation between adjacent bands equal to $3.1\,nm$, is demonstrated, which is highly appealing and promising for all-optical devices, such as dense wavelength-division-multiplexed (DWDM) system, multi-wavelength fiber lasers, and fiber-optic sensors.

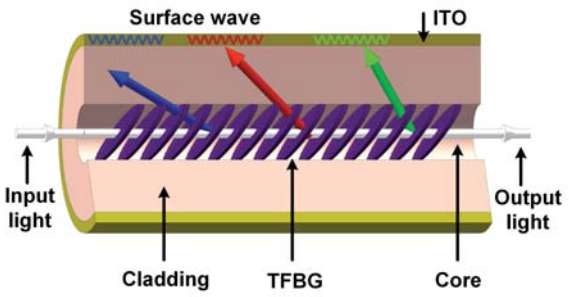

Figure 1: Schematic of comb-like polarizer based on ITO integrated TFG.

2. Design and Principle

The sketch of the polarizer consisting of the TFG with ITO nanocoating is shown in Fig. 1.

A standard Corning SMF-28e+ single mode fiber with core radius of 4.1 μm and cladding radius of 62.5 μm is considered. The refractive index of fiber cladding n_{cl}, made of fused silica, is estimated using the Sellmeier equation [35]. The refractive index of the fiber core n_{co} is then obtained by increasing n_{cl} by 0.36% according to the specifications from Corning Inc. The external environment is assumed to be air with surrounding refractive index (SRI) of 1.0.

The ITO nanocoating is taken into account to tune the mode characteristics and resonance spectrum of the TFG. At the near infrared wavelength where the TFG works, the ITO nanocoating is a high refractive index material with large real part of the refractive index and a small imaginary part. Many precisely controlled deposition techniques like magnetron sputtering and sol-gel dip-coating have been reported to deposit uniform and smooth ITO nm-thick overlay on optical fibers [36, 37]. In these cases, the theoretical optimizations agree very well with the experimental results. In this work, the experimental data of optical constants of the ITO nanocoating are extrapolated from Ref. [36].

The PMC is an important tool to determine the resonance modes interacting with the core mode in the TFG, which is given by [23]:

$$\lambda_i = Re\left(n_{eff}^{co} + n_{eff}^{i}\right)\Lambda = Re\left(n_{eff}^{co} + n_{eff}^{i}\right)\frac{\Lambda_g}{\cos\theta} \quad (1)$$

in which λ_i represents the resonance wavelength, n_{eff}^{co} the effective refractive index (ERI) of the core mode, n_{eff}^{i} the ERI of the ith fiber mode including the cladding mode and leaky mode, Λ the axial grating period, Λ_g the normal period of index perturbation plane, and θ the tilt angle. According to the PMC, the larger the tilt angle θ, the smaller the ERI n_{eff}^{i}, indicating that high order modes can be excited at larger tilt angle. When the TFG operates in air environment with surrounding RI being about 1.0, the leaky modes have the ERI smaller than 1.0. Therefore, in order to excite the leaky modes corresponding to higher order fiber modes and according to the PMC given in Eq. (1), the index perturbation plane is angled at 26.5° with respect to the fiber axis. It is worth pointing out that this value of tilt angle represents the optimized one even if other values can excite leaky modes. In fact, tilt angles larger than 26.5° would lead to a shift of the resonances towards shorter wavelengths, while tilt angle smaller than 26.5° would lead to a transmission spectrum consisting of both leaky and cladding mode resonances with very weak polarization selectivity. The tilted grating can be inscribed in the fiber core using ultraviolet laser irradiation that is a mature technology. Another recent but very promising approach to fabricate TFGs concerns the use of femtosecond laser sources [38]. In the present analysis, axial grating period Λ of $550\,nm$ and index modulation amplitude of 6.0×10^{-4} will be taken into account.

At the tilted grating region, the forward prop-

agating core mode couples with the backward propagating fiber modes that satisfy the PMC, yielding the transmission spectrum given by [23]:

$$T \approx 1 - \tanh^2(\kappa L) \tag{2}$$

where κ is the coupling coefficient and L is the grating length. The transmission spectrum can be calculated using the classical full-vector coupled mode theory that is detailed in Ref. [39]. As highlighted in Eq. (2), the resonance amplitude substantially depends on two factors including κ and L. Generally for the guided modes, like the core mode and cladding modes, there is an extremely small mode loss that is closely related to the imaginary component of the ERI. This means the guided modes can propagate along the waveguide with negligible attenuation. In this case, full interaction between guided modes is obtained and hence the corresponding transmission can accurately be simulated using these two factors: κ and L.

However, it is important to remark that the mode loss plays a significant role in the mode coupling when the leaky modes contribute to the transmission spectrum. It has been demonstrated that the leaky modes (both TE and TM cases) have a larger coupling coefficient κ than that of cladding modes but they still present an extremely weak resonance in bare TFG [32]. This is because they are highly lossy modes that show a very large imaginary part of ERI and a real component smaller than that of surrounding environment. Due to its high lossy property, the leaky modes always radiate immediately out of the fiber cladding, indicating that they cannot effectively interact with the core mode. Consequently, an extremely weak resonance is obtained in bare TFG. When the ITO nanocoating is considered, the lossy property becomes highly polarization-dependent due to the mode transition, especially for the leaky modes. The increased difference in dispersion property between TE and TM modes makes the resonance spectrum being highly polarization-dependent and increases the spectrum contrast, which greatly benefits for the realization of linear polarizers.

3. Results and Discussion

3.1. Nanocoating Induced Polarization Property

The evolution of the ERI with the ITO thickness at $\lambda = 1.55\,\mu m$ is depicted in Fig. 2. Here the $TE/TM_{0,m}$ modes that always exist in pairs are considered for illustration. The modes are numbered in sequence from $m = 1$ and some modes are marked in this figure to get a clear comparison. In this sense, the $TE/TM_{0,84}$ is the last cladding mode and the $TE/TM_{0,85}$ corresponds to the first leaky mode (see Fig. 2(a)). There are two kinds of leaky modes [40]: guided-like leaky modes marked as G-leaky modes and radiation-like leaky modes represented by R-leaky modes, as shown in Fig. 2(a). Both of them have the real component of ERI smaller than the SRI but the R-leaky modes are more highly lossy as com-

pared with the G-leaky counterparts (evidenced by a much larger imaginary part of ERI).

One of the most expressive signatures drawn from Fig. 2(a) is the phenomenon of mode transition after integration of the ITO nanocoating. Of this configuration, the mode transition of lower order modes that are the cladding modes have been widely reported for the generation of lossy mode resonance (L^{o}MR) [12]. On the other hand, this work pays the attention on the higher order modes corresponding to the leaky modes.

As illustrated in Fig. 2(a), the cladding modes and G-leaky modes are characterized by the same variation trend, presenting a progressive increase of the real component of ERI with the ITO thickness (combined with a periodic small fluctuation between TE and TM modes). In contrast, the R-leaky modes exhibit an opposite variation, i.e., the real part of ERI decreases slightly with the ITO thickness. During the variation, two kinds of mode transitions are clearly observed for the first several leaky modes: one corresponds to the transition between the G-leaky modes and the R-leaky modes, and the other is the process from the leaky modes to the cladding modes. For instance, the $TM_{0,88}$ G-leaky (and $TM_{0,87}$ R-leaky) mode becomes the $TM_{0,87}$ R-leaky (and $TM_{0,88}$ G-leaky) mode at specific ITO thickness ($\sim 50\,nm$) and similar transition occurs again at thickness of $\sim 200\,nm$. When the ITO thickness increases to $\sim 300\,nm$, the first leaky mode corresponding

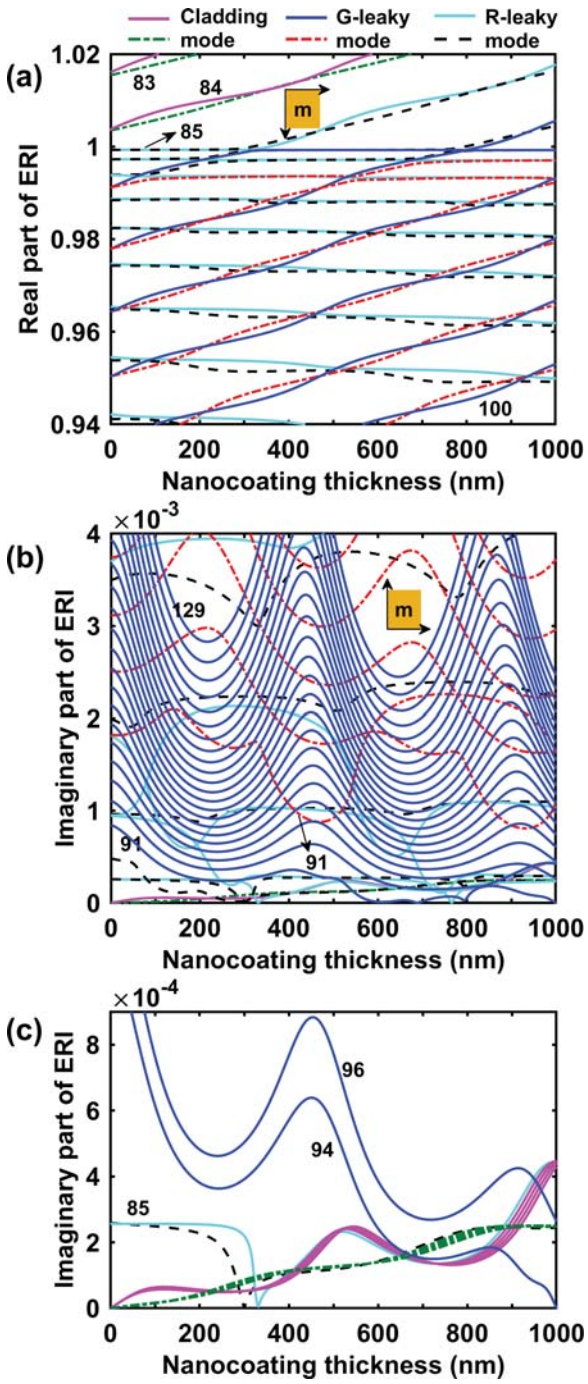

Figure 2: Evolution of effective refractive index with ITO thickness: (a) Real part, (b) Imaginary part, and (c) Imaginary part of selected modes. Solid and dash lines represent TE and TM modes, respectively.

to $TE/TM_{0,85}$ becomes the last cladding mode, which is clearly evidenced by the increased real part of ERI that becomes larger than the SRI. In the meanwhile, the adjacent G-leaky mode takes the place of original $TE/TM_{0,85}$ mode and becomes the first R-leaky mode. It is remarkable to note that these two kinds of transition processes occur quasi-periodically as the ITO thickness increases continuously. This means that more G-leaky modes gradually become these modes that present larger ERI (real part) and are finally turned into the cladding modes. Generally, these modes with larger ERI (real part) are better confined in the optical fiber, and hence exhibit smaller mode loss. Meanwhile, the ERI (real part) of R-leaky modes decreases with the ITO thickness allowing these modes to become more lossy as compared with the bare case.

The imaginary component of ERI depicted in Fig. 2(b) gives a clear illustration on the polarization-dependent property of the variation of mode characteristics. The ERI of R-leaky modes (except for the first few R-leaky modes) is much larger than that of G-leaky counterparts and it is not shown in this figure. A quasi-periodic property is observed for both TE and TM G-leaky modes, but they present considerably different variation trend. It can also be observed that the ERI of TE modes decreases firstly and then increases with the ITO thickness changing from $0\,nm$ to $\sim 500\,nm$, which approximately corresponds to a periodic variation process. In the meanwhile, however, an opposite variation is obtained in a period for the TM modes. For instance at thickness of $\sim 235\,nm$, the TE modes exhibit a minimum ERI (imaginary part) but a maximum value is obtained for the TM counterparts. It should be mentioned that the higher order TM modes also present a great reduction of ERI (compared with bare case), which is shown in Fig. 3 below.

The ERI evolution of few modes is plotted in Fig. 2(c) where the mode transition can be obviously identified. Compared with Fig. 2(a), the ERI (imaginary component) of the $85th$ R-leaky mode decreases sharply to near 0 at the transition point ($\sim 300\,nm$) and then varies with the ITO thickness in the same manner as that of the corresponding cladding modes. This clearly demonstrates the transition from leaky modes to cladding modes. When the ITO thickness continuously increases, the mode transition occurs for the higher order leaky modes like the $94/96th$ G-leaky modes at thickness of $\sim 1000\,nm$.

3.2. Guidance of Leaky Modes

Figure 3 compares the variation of ERI by considering bare TFG and $235\,nm$-ITO coated TFG. From the figure, it is clear that even TE and TM modes of bare TFG present large difference in the ERI (high polarization selectivity might be obtained), but with a very large imaginary part of the ERI for both modes (indicating that both of them cannot be effectively guided in bare TFG),

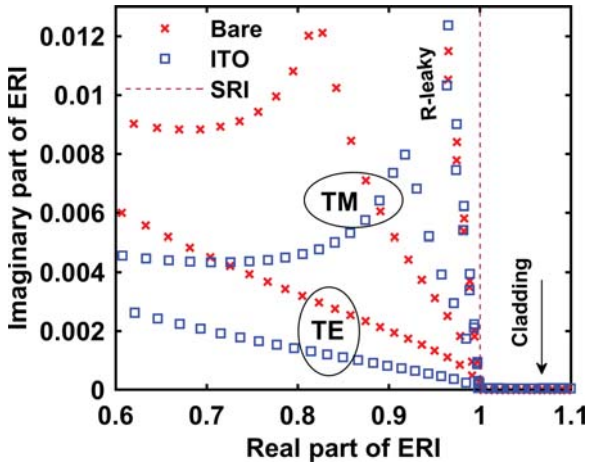

Figure 3: Variation of effective refractive index of bare TFG and of 235 nm-ITO coated TFG.

which leads to extremely weak resonances in the transmission spectrum. Therefore, it turns out that bare TFGs can be barely used as comb-like linear polarizer with high polarization extinction ratio. After integrating the ITO nanocoating, the ERI (imaginary part) of both TE and TM modes is greatly reduced, except for the first several TM G-leaky modes. However, it is important to highlight that the reduced ERI of higher order TM modes is still even larger than that of the TE modes of bare TFG, which clearly indicates that the TM leaky modes are always highly lossy. This can be verified by the confinement loss that is defined as $\alpha = 8.686 \times 2\pi/\lambda \times |\mathrm{Im}\,(n_{eff})\,|$ [41]. As clearly shown in Fig. 4, the TE G-leaky modes present a much smaller loss than that of the TM counterparts. The smaller loss gives rise to a longer propagation length, indicating that the TE G-leaky modes become guided in the ITO coated TFG. Therefore, the guidance of TE leaky modes will lead to a much stronger interaction with the core mode, as compared with the bare TFG.

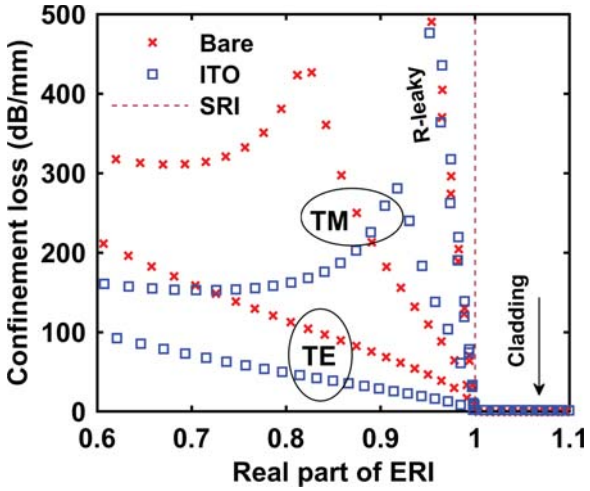

Figure 4: Variation of confinement loss of bare TFG and of 235 nm-ITO coated TFG.

3.3. Polarized Leaky Mode Resonance

Figure 5 shows the polarized spectrum of the TFG coated with the ITO nm-thick overlay with different thicknesses. The grating length is 20 mm and other parameters are indicated above. As for the bare TFG, there are very weak resonance bands corresponding to both cladding modes and leaky modes in both TE and TM polarized spectra. The resonance of TE leaky modes is somewhat stronger than that of TM modes. This is because of that the TE leaky modes present a smaller imaginary part of ERI (or mode loss).

The mode transition induced by the ITO nanocoating leads to a significant variation of the TE L^{e}MR, resulting in eL^{e}MR. It can be clearly observed that with the increase of the ITO thickness, the eL^{e}MR is obtained in the TE polarized spectrum

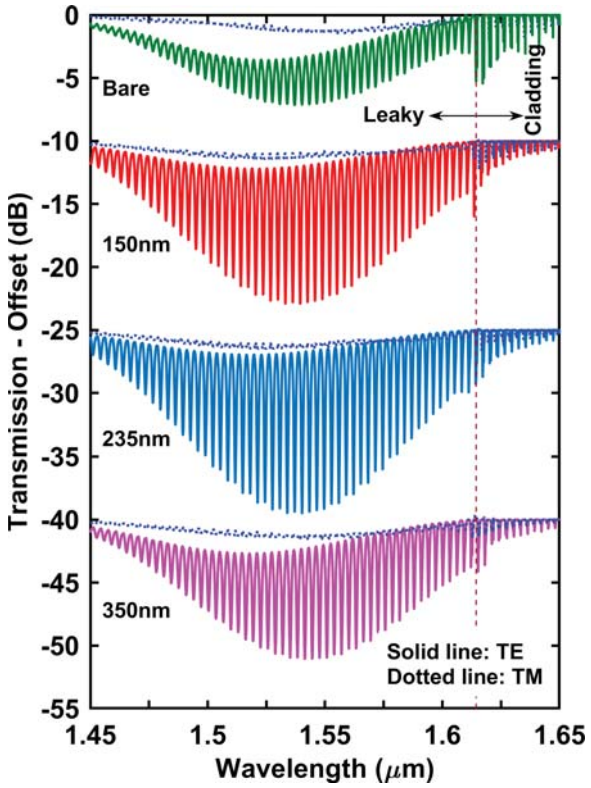

Figure 5: Evolution of polarized transmission with nanocoating thickness.

while the TM-related resonance shows negligible change, and hence any eL^{e}MR can be yielded for this polarization. Apparently, the 235 nm-ITO nanocoating induces the strongest TE eL^{e}MR, which gives rise to the highest contrast between the TE and TM spectra. The continuous increase of the ITO thickness weakens the eL^{e}MR like the case of 350 nm. In this sense, the 235 nm-ITO nanocoating is considered in the following discussion. The spectrum variation obtained in Fig. 5 agrees well with the evolution of mode characteristics shown in Fig. 2. Compared with the results obtained above, it is obvious that the guidance of TE G-leaky modes after integrating the ITO nanocoating plays a key role in the generation of the eL^{e}MR. For instance, the strongest TE eL^{e}MR occurs at 235 nm-ITO nanocoating, the thickness at which the smallest ERI (imaginary component) is also obtained. In addition, the negligible change of the TM spectrum can be attributed to the fact that the TM G-leaky modes are highly lossy and hence they cannot fully interact with the core mode. Therefore, it is the difference in the dispersion property of the involved materials that leads to the polarization-dependent feature in the transmission spectrum of the TFG with ITO nanocoating.

Moreover, according to the PMC highlighted in Eq. (1), the resonance dip in the spectrum is generated at the wavelength where the mode coupling occurs whereas the resonance peak exists at the wavelength where the mode dissatisfies the PMC (i.e., out of the PMC condition). Consequently, the incident TE light at resonance dip is coupled into the TE G-leaky modes that can propagate backward along the ITO coated TFG while the light at resonance peak propagates forward along this configuration. In the meanwhile, the extremely weak TM L^{e}MR means that the incident TM light can propagate directly through the TFG since it cannot fully interact with the TM G-leaky modes that are highly lossy. Therefore, the incident unpolarized light can be separated into two orthogonal linearly polarized components at the resonance dip: one corresponds to the forward propagating TM light and the other is the back-

ward propagating TE light that can be collected using an optical circulator. In addition, in view of the dense comb-like eL^{e}MR excited by the ITO nanocoating, it is obvious that the eL^{e}MR can be used to realize an in-fiber comb-like linear polarizer.

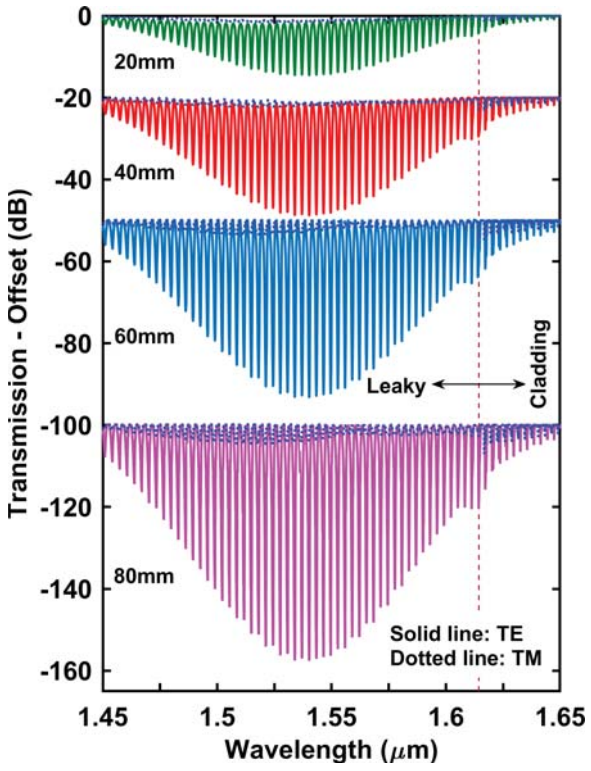

Figure 6: Evolution of polarized transmission with grating length.

A simple approach can be used to further optimize the polarizer performance, that is, increasing the grating length. Indeed the resonance amplitude depends on two factors including the coupling coefficient κ and grating length L, according to Eq. (2). However, it is very difficult to increase the factor κ since it is strongly determined by the refractive index modulation (a strong modulation in the TFG should be inscribed). In Fig. 6, the spectrum is represented for four grating lengths while maintaining the other parameters. It can be clearly observed that the TE eL^{e}MR is significantly improved with the increase of grating length while there is very small variation for the TM L^{e}MR. The improved eL^{e}MR apparently offers two advantages: (1) more power of the incident light is coupled into the backward light to increase the spectrum contrast between TE and TM polarization states, and (2) a narrower FWHM can be obtained for the polarizer. In addition, the improved eL^{e}MR gives rise to the increase of polarization dependent loss (PDL) that is defined as [42]:

$$PDL\left(\lambda\right) = \left|10 \times \log\left(\frac{T_{TM}\left(\lambda\right)}{T_{TE}\left(\lambda\right)}\right)\right| \qquad (3)$$

in which $T(\lambda)$ represents the two orthogonal polarization spectra. The evolution of the PDL with the grating length is depicted in Fig. 7. It can be seen that the L^{e}MR presents a smooth PDL envelope for the $20\,mm$ and $40\,mm$ TFGs. This is due to a relatively small spectral contrast between the two orthogonal polarization states. Moreover, the smooth envelope confirms that the TE eL^{e}MR and TM L^{e}MR have the same resonance wavelength with each other (the peaks/dips in the PDL envelope correspond to the resonance dips/peaks in the transmission spectrum in Fig. 6). The cladding mode resonance shows a PDL with a great number of perturbations. This is because the TE and TM spectra differ in the resonance wavelengths, especially for the higher order cladding

modes close to the cut-off wavelength. Here only the PDL of L^{e}MR is analyzed for the polarizer. When the grating length becomes longer than 40 mm, a higher PDL is obtained but combined with peaks close to the corresponding PDL dips. A closer comparison with Fig. 6 reveals that these peaks occur nearly at the same wavelengths of the resonance peaks in the transmission spectrum where the amplitude of the TE eL^{e}MR equals approximately to 0. We focus here on the variation of the PDL envelope. It is interesting to see that the maximum PDL envelope exists at around 1.55 μm and it changes from 11.6 dB for the 20 mm TFG to 29.2 dB for the 80 mm TFG, a great enhancement for a polarizer.

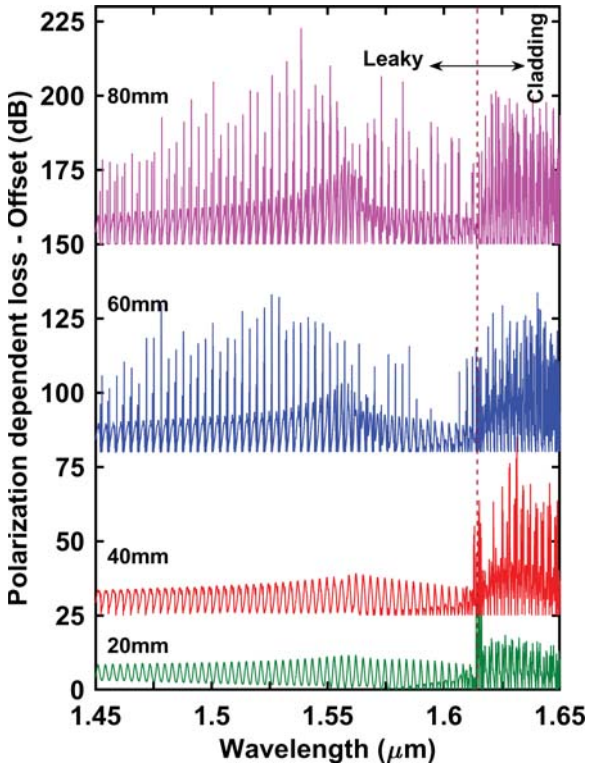

Figure 7: Variation of polarization dependent loss with grating length.

In order to analyze the polarization performance, the evolution of polarized transmission with the polarization angle of incident light is depicted in Fig. 8 where 20 mm and 80 mm TFGs with 235 nm-ITO nanocoating are taken into account. It can be seen that the L^{e}MR is characterized by an obvious periodic variation in the resonance amplitude with the polarization angle, presenting a period of 90 degrees, while the resonance wavelength keeps constant. It is evident that there are two identical symmetric sets of resonances with the spectrum density centered at the angles of 90° and 270°, respectively, where the highest amplitude is obtained. In this case, the light is tuned into one linear polarization state, which is actually the TE state. However, these resonances almost disappear at the angles of 0°, 180° and 360°, indicating another linear polarization case corresponding to the TM state is reached. In addition, the 80 mm TFG presents a smaller resonance area (along the horizontal axis; wavelength) for each resonance band than that of 20 mm TFG, which confirms the bandwidth can be narrowed by increasing the grating length. It is also clear that the eL^{e}MR bands are separated each other with the wavelength separation equal to 3.1 nm and without crosstalk induced by adjacent bands in a broad wavelength range.

A detailed comparison between the L^{e}MR and cladding mode resonance is provided in Fig. 8(c). It is interesting to notice that the cladding modes

show an obvious periodic change both in the resonance amplitude and wavelength with the polarization angle, which is indicated by a periodic evolution of the spectral density along the horizontal and vertical axes. This is because there is a relatively small spectrum contrast but with a large difference in wavelength between the TE and TM cladding mode resonances. As for the L^{e}MR, a much smaller resonance area is observed, while the resonance wavelength remains constant.

As an example of the polarization property of the designed polarizer, Fig. 9 accounts for the polarization response of three L^{e}MRs around three wavelengths for the 20 mm and 80 mm TFGs. It can be seen that the polarization response is expected to be characterized by a nearly perfect '8' shape at all three wavelengths, but the 80 mm TFG with improved eL^{e}MR presents a much larger response range than the case of 20 mm TFG. The '8' shape behavior indicates the linear polarization property of the designed polarizer. At around 1.54 μm where the strongest eL^{e}MR exists, the polarization response shows the highest contrast, indicated by the amplitude changing from near 0 dB at polarization angle 0° to 57 dB at 90°, which is a considerably large contrast. At other wavelengths like 1.50 μm (or 1.60 μm) the contrast is decreased to about 42 dB (or 22 dB) but it is still much higher than the bare TFG. Compared with Fig. 6, a high contrast more than 20 dB can be obtained over a wavelength range of about

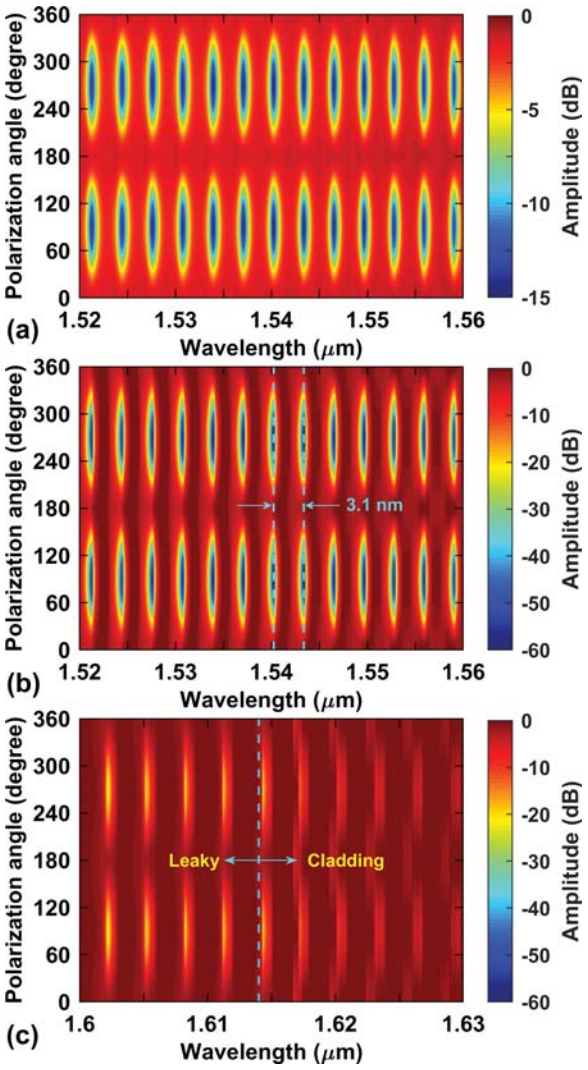

Figure 8: Spectral density evolution of polarized transmission with polarization angle of incident light: (a) leaky mode resonance of 20 mm TFG, (b) leaky mode resonance of 80 mm TFG, and (c) leaky mode resonance and cladding mode resonance of 80 mm TFG.

$140\,nm$ (from $\sim 1475\,nm$ to $\sim 1615\,nm$). Moreover, it is remarkable to highlight that the TFG can be designed to work at other wavelengths by readily tailoring its parameters like the grating period and tilt angle. This means that the operating wavelength of the polarizer can be tuned in a large range. For instance, a much wider spectrum can be attained by inscribing the TFG with multiple tilt angles [43].

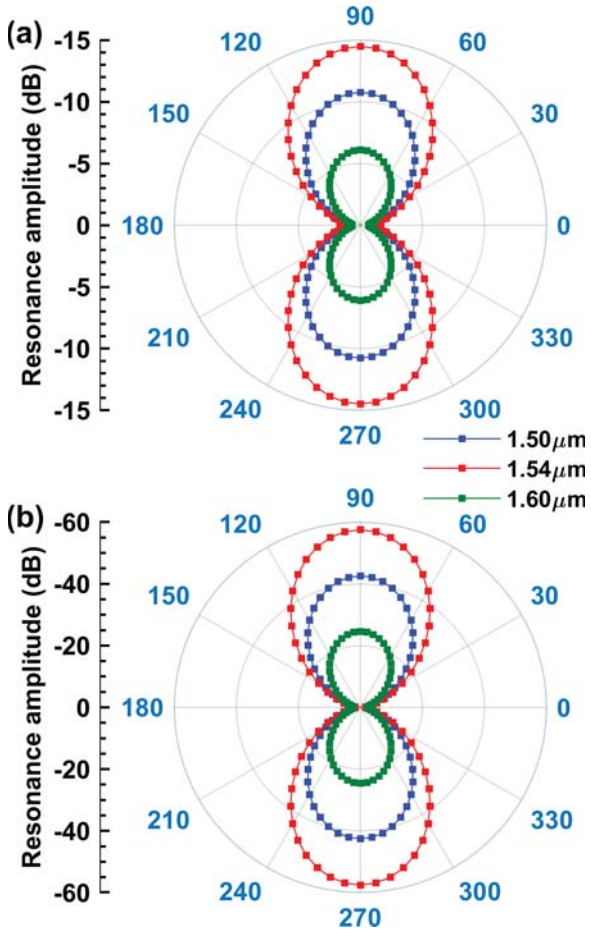

Figure 9: Polarization response of (a) $20\,mm$ TFG and (b) $80\,mm$ TFG with $235\,nm$-ITO nanocoating.

3.4. Linear Comb-like Polarizer

The performance of the designed polarizer is detailed in Fig. 10. The PER is defined as the difference between the minimum and maximum resonance intensities [25, 28]. Therefore, PER has been calculated by $PER(\lambda) = T_{\min}(\lambda) - T_{\max}(\lambda)$ with T_{min}/T_{max} representing the minimum/maximum resonance amplitude, which actually corresponds to the resonance contrast in Fig. 9. From Fig. 10 it is worth pointing out that with this design the polarization performance can significantly be improved. The bare TFG presents a very small PER combined with a larger FWHM due to the weak L^{e}MR. After the integration of the $235\,nm$-ITO nanocoating, the mode transition leads to the TE eL^{e}MR, and hence the PER and the FWHM are improved greatly. A significant enhancement can be obtained by simply increasing the grating length. As far as the $80\,mm$ TFG is concerned, the improved eL^{e}MR permits to reach a PER up to $57\,dB$ and a FWHM smaller than $0.5\,nm$, which is a considerable performance improvement for fiber-optic polarizers.

The best performance could be maintained in real applications that might suffer from the insertion loss. Since the key component of the in-fiber linear polarizer is the thin film coated TFG that can be readily inscribed in standard single mode fibers by mature technology based on ultraviolet laser irradiation, the insertion loss mainly comes from two aspects: splicing loss and scattering loss. While the splicing loss between single mode fibers (the TFG and fiber pigtails) can be greatly decreased using a commercial fusion

splicer, the scattering loss depends on the uniformity of the ITO thin film deposited onto the fiber surface. Many techniques like sol-gel–based dip-coating and magnetron sputtering can be used to deposit uniform, smooth and precisely-controlled nanometric films, thus proving that the experimental results agree with the theoretical predictions [36, 37]. Therefore, it can reasonably assert that the features of the in-fiber comb-like linear polarizer attained with remarkable performance can be also obtained experimentally.

4. Conclusion

In conclusion, we propose and theoretically investigate an in-fiber comb-like polarizer based on the enhanced leaky mode resonance (eL^{e}MR) in tilted fiber grating (TFG) coated with indium tin oxide (ITO) nm-thick overlay in this work. The ITO film with a high refractive index induces a quasi-periodic leaky mode transition encompassing two processes: one is the transition from the leaky modes to the cladding modes, and the other corresponds to the transition between the guided-like leaky (G-leaky) modes and the radiation-like leaky (R-leaky) modes. The mode transition leads to a significant polarization-dependent variation of the leaky mode features, indicated by a great change of the imaginary part of effective refractive index (ERI). The analysis shows that the TE-polarized G-leaky modes that are highly lossy in bare TFG present the smallest ERI (imagi-

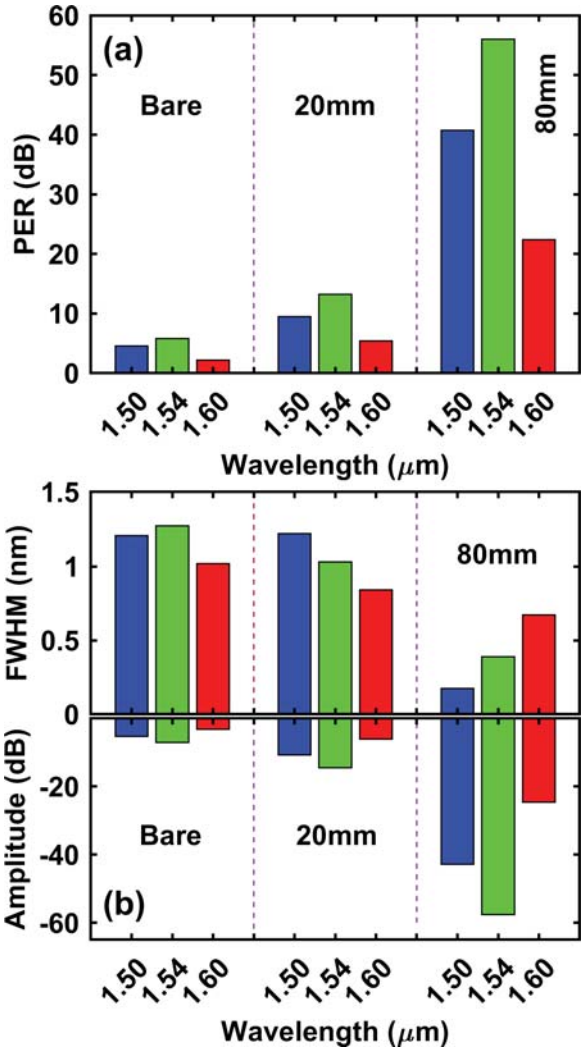

Figure 10: (a) Polarization extinction ratio and (b) bandwidth (top) and amplitude (bottom) of bare TFG and ITO coated TFG.

nary part) and mode loss at the ITO thickness of about 235 nm (much smaller than that of the TM G-leaky modes). This indicates the TE G-leaky modes become guided in the TFG with ITO nanocoating. As a consequence, the guidance of leaky modes gives rise to a full interaction with the core mode, which leads to the generation of the TE eL^{e}MR. In contrast, the TM L^{e}MR is always extremely weak due to the highly lossy property of the TM G-leaky modes, and hence any eL^{e}MR can be yielded for this polarization.

Later on, the eL^{e}MR can be designed to realize an in-fiber comb-like polarizer with high polarization extinction ratio (PER) and narrow bandwidth at wide wavelength range. By simply increasing the grating length, the eL^{e}MR can be further improved to increase the resonance contrast between the TE and TM spectra. This permits to significantly optimize the linear polarization performance of the designed polarizer, with the results demonstrating that a PER up to 57 dB and a bandwidth smaller than 0.5 nm can be attained. The high contrast between TE and TM eL^{e}MRs offers the capability of linear polarization output and the narrow bandwidth accompanied with a considerable separation between adjacent bands provides advantages of decreasing or even removing the crosstalk, which are highly appealing and promising for all-optical devices like the DWDM system and multi-wavelength fiber lasers without additional wavelength selection devices. In addition, by tailoring the parameters, like the grating period and tilt angle of the TFG, it is possible to tune the operating wavelength of the polarizer in a wide window.

Moreover, considering that the ITO is a typical metal oxide having high refractive index combined with a much smaller imaginary part, it is expected that the dense comb-like eL^{e}MR bands can also be excited by other metal oxide nano-films with similar dispersion property, such as titanium dioxide (TiO_2), indium oxide (In_2O_3), tin-dioxide (SnO_2), aluminum doped zinc oxide (AZO), zinc oxide (ZnO), aluminum oxide (Al_2O_3), and even some polymers. This is a very interesting phenomenon and some new tunable features could be attained depending on the photo-electronic properties of these materials. This study is expected to open up new opportunities for eL^{e}MR-based in-fiber devices and provide some guidelines for future research in the field.

References

[1] W. Eickhoff, In-line fibre-optic polariser, Electron. Lett. 16 (20) (1980) 762–764. doi:10.1049/el:19800541.

[2] R. A. Bergh, H. C. Lefevre, H. J. Shaw, Single-mode fiber-optic polarizer, Opt. Lett. 5 (11) (1980) 479–481. doi:10.1364/OL.5.000479.

[3] S. G. Lee, J. P. Sokoloff, B. P. McGinnis, H. Sasabe, Fabrication of a side-polished fiber polarizer with a birefringent polymer overlay, Opt. Lett. 22 (9) (1997) 606–608. doi:10.1364/OL.22.000606.

[4] C.-H. Dong, C.-L. Zou, X.-F. Ren, G.-C. Guo, F.-

W. Sun, In-line high efficient fiber polarizer based on surface plasmon, Appl. Phys. Lett. 100 (4) (2012) 041104. doi:10.1063/1.3678591.

[5] J. R. Feth, C. L. Chang, Metal-clad fiber-optic cutoff polarizer, Opt. Lett. 11 (6) (1986) 386–388. doi:10.1364/OL.11.000386.

[6] F. Zhou, W. Du, A graphene-based all-fiber TE/TM switchable polarizer, J. Opt. 20 (3) (2018) 035401. doi:10.1088/2040-8986/aaa6fa.

[7] Q. Bao, H. Zhang, B. Wang, Z. Ni, C. H. Y. X. Lim, Y. Wang, D. Y. Tang, K. P. Loh, Broadband graphene polarizer, Nat. Photonics 5 (7) (2011) 411–415. doi:10.1038/nphoton.2011.102.

[8] A. Zubair, D. E. Tsentalovich, C. C. Young, M. S. Heimbeck, H. O. Everitt, M. Pasquali, J. Kono, Carbon nanotube fiber terahertz polarizer, Appl. Phys. Lett. 108 (14) (2016) 141107. doi:10.1063/1.4945708.

[9] H. Zhang, N. Healy, L. Shen, C. C. Huang, N. Aspiotis, D. W. Hewak, A. C. Peacock, Graphene-Based Fiber Polarizer With PVB-Enhanced Light Interaction, J. Lightwave Technol. 34 (15) (2016) 3563–3567. doi:10.1109/JLT.2016.2581315.

[10] R. Chu, C. Guan, J. Yang, Z. Zhu, P. Li, J. Shi, P. Tian, L. Yuan, G. Brambilla, High extinction ratio D-shaped fiber polarizers coated by a double graphene/PMMA stack, Opt. Express 25 (12) (2017) 13278–13285. doi:10.1364/OE.25.013278.

[11] Ssu-Pin Ma, Shiao-Min Tseng, High-performance side-polished fibers and applications as liquid crystal clad fiber polarizers, J. Lightwave Technol. 15 (8) (1997) 1554–1558. doi:10.1109/50.618389.

[12] I. Del Villar, F. J. Arregui, C. R. Zamarreño, J. M. Corres, C. Bariain, J. Goicoechea, C. Elosua, M. Hernaez, P. J. Rivero, A. B. Socorro, A. Urrutia, P. Sanchez, P. Zubiate, D. Lopez, N. De Acha, J. Ascorbe, I. R. Matias, Optical sensors based on lossy-mode resonances, Sensor. Actuat. B Chem. 240 (2017) 174–185. doi:10.1016/j.snb.2016.08.126.

[13] Q. Bao, K. P. Loh, Graphene Photonics, Plasmonics, and Broadband Optoelectronic Devices, ACS Nano 6 (5) (2012) 3677–3694. doi:10.1021/nn300989g.

[14] M. Liu, X. Yin, E. Ulin-Avila, B. Geng, T. Zentgraf, L. Ju, F. Wang, X. Zhang, A graphene-based broadband optical modulator, Nature 474 (7349) (2011) 64–67. doi:10.1038/nature10067.

[15] A. Vakil, N. Engheta, Transformation Optics Using Graphene, Science 332 (6035) (2011) 1291–1294. doi:10.1126/science.1202691.

[16] C. Guan, S. Li, Y. Shen, T. Yuan, J. Yang, L. Yuan, Graphene-Coated Surface Core Fiber Polarizer, J. Lightwave Technol. 33 (2) (2015) 349–353. doi:10.1109/JLT.2014.2386893.

[17] Y. Wang, L. Xiao, D. N. Wang, W. Jin, In-fiber polarizer based on a long-period fiber grating written on photonic crystal fiber, Opt. Lett. 32 (9) (2007) 1035–1037. doi:10.1364/OL.32.001035.

[18] P. Romagnoli, C. R. Biazoli, M. A. R. Franco, C. M. B. Cordeiro, C. J. S. de Matos, Integrated polarizers based on tapered highly birefringent photonic crystal fibers, Opt. Express 22 (15) (2014) 17769–17775. doi:10.1364/OE.22.017769.

[19] W. Qian, C.-L. Zhao, Y. Wang, C. C. Chan, S. Liu, W. Jin, Partially liquid-filled hollow-core photonic crystal fiber polarizer, Opt. Lett. 36 (16) (2011) 3296–3298. doi:10.1364/OL.36.003296.

[20] X. Zhang, R. Wang, F. M. Cox, B. T. Kuhlmey, M. C. J. Large, Selective coating of holes in microstructured optical fiber and its application to in-fiber absorptive polarizers, Opt. Express 15 (24) (2007) 16270–16278. doi:10.1364/OE.15.016270.

[21] S. Ramachandran, M. Das, Z. Wang, J. Fleming, M. Yan, High extinction, broadband polarisers using long-period fibre gratings in few-mode fibres, Electron. Lett. 38 (22) (2002) 1327. doi:10.1049/el:20020926.

[22] C. Zou, Q. Huang, T. Wang, Z. Yan, M. AlAraimi,

A. Rozhin, C. Mou, Single/dual-wavelength switchable bidirectional Q-switched all-fiber laser using a bidirectional fiber polarizer, Opt. Lett. 43 (19) (2018) 4819–4822. doi:10.1364/OL.43.004819.

[23] J. Albert, L.-Y. Shao, C. Caucheteur, Tilted fiber Bragg grating sensors, Laser Photonics Rev. 7 (1) (2013) 83–108. doi:10.1002/lpor.201100039.

[24] C. Caucheteur, T. Guo, J. Albert, Polarization-assisted fiber Bragg grating sensors: Tutorial and review, J. Lightwave Technol. 35 (16) (2017) 3311–3322. doi:10.1109/JLT.2016.2585738.

[25] K. Zhou, G. Simpson, X. Chen, L. Zhang, I. Bennion, High extinction ratio in-fiber polarizers based on 45° tilted fiber Bragg gratings, Opt. Lett. 30 (11) (2005) 1285–1287. doi:10.1364/OL.30.001285.

[26] H. Qin, Q. He, Y. Moreno, Z. Xing, X. Guo, Z. Yan, Q. Sun, K. Zhou, D. Liu, L. Zhang, Compact linear polarization spectrometer based on radiation mode shaped in-fiber diffraction grating, Opt. Lett. 44 (21) (2019) 5129–5132. doi:10.1364/OL.44.005129.

[27] Z. Yan, C. Mou, H. Wang, K. Zhou, Y. Wang, W. Zhao, L. Zhang, All-fiber polarization interference filters based on 45°-tilted fiber gratings, Opt. Lett. 37 (3) (2012) 353–355. doi:10.1364/OL.37.000353.

[28] Z. Yan, K. Zhou, L. Zhang, In-fiber linear polarizer based on UV-inscribed 45° tilted grating in polarization maintaining fiber, Opt. Lett. 37 (18) (2012) 3819–3821. doi:10.1364/OL.37.003819.

[29] Z. Yan, C. Mou, K. Zhou, X. Chen, L. Zhang, UV-Inscription, Polarization-Dependant Loss Characteristics and Applications of 45° Tilted Fiber Gratings, J. Lightwave Technol. 29 (18) (2011) 2715–2724. doi:10.1109/JLT.2011.2163196.

[30] G. Yin, S. Lou, Q. Li, H. Zou, Theory analysis of mode coupling in tilted long period fiber grating based on the full vector complex coupled mode theory, Opt. Laser Technol. 48 (2013) 60–66. doi:10.1016/j.optlastec.2012.10.002.

[31] Z. Yan, H. Wang, C. Wang, Z. Sun, G. Yin, K. Zhou, Y. Wang, W. Zhao, L. Zhang, Theoretical and experimental analysis of excessively tilted fiber gratings, Opt. Express 24 (11) (2016) 12107–12115. doi:10.1364/OE.24.012107.

[32] Z. Li, X. Ruan, Y. Dai, Leaky Mode Combs in Tilted Fiber Bragg Grating, J. Lightwave Technol. 37 (24) (2019) 6165–6173. doi:10.1109/JLT.2019.2947251.

[33] Z. Li, X. Ruan, Y. Dai, Simultaneous excitation of leaky mode resonance and surface plasmon resonance in tilted fiber Bragg grating, Appl. Phys. Express 12 (11) (2019) 112005. doi:10.7567/1882-0786/ab49a3.

[34] Z. Li, Q. Bao, J. Zhu, X. Ruan, Y. Dai, Generation of leaky mode resonance by metallic oxide nanocoating in tilted fiber-optic gratings, Opt. Express 28 (7) (2020) 9123–9135. doi:10.1364/OE.389363.

[35] R. Kashyap, Fiber Bragg Gratings, 2nd Edition, Academic Press, MA, USA, 2010.

[36] F. Chiavaioli, P. Zubiate, I. Del Villar, C. R. Zamarreño, A. Giannetti, S. Tombelli, C. Trono, F. J. Arregui, I. R. Matias, F. Baldini, Femtomolar Detection by Nanocoated Fiber Label-Free Biosensors, ACS Sens. 3 (5) (2018) 936–943. doi:10.1021/acssensors.7b00918.

[37] I. D. Villar, C. R. Zamarreno, M. Hernaez, F. J. Arregui, I. R. Matias, Lossy Mode Resonance Generation With Indium-Tin-Oxide-Coated Optical Fibers for Sensing Applications, J. Lightwave Technol. 28 (1) (2010) 111–117. doi:10.1109/JLT.2009.2036580.

[38] A. Ioannou, A. Theodosiou, C. Caucheteur, K. Kalli, Direct writing of plane-by-plane tilted fiber bragg gratings using a femtosecond laser, Opt. Lett. 42 (24) (2017) 5198–5201. doi:10.1364/OL.42.005198.

[39] Y.-C. Lu, W.-P. Huang, S.-S. Jian, Full vector complex coupled mode theory for tilted fiber gratings, Opt. Express 18 (2) (2010) 713–726. doi:10.1364/OE.18.000713.

[40] Z. Li, X. Shen, Y. Hua, X. Ruan, Y. Dai, Leaky mode transition and enhanced resonance in tilted fiber Bragg grating, J. Appl. Phys. 126 (15) (2019) 154501. doi:10.1063/1.5121904.

[41] B. T. Kuhlmey, H. C. Nguyen, M. J. Steel, B. J. Eggleton, Confinement loss in adiabatic photonic crystal fiber tapers, J. Opt. Soc. Am. B 23 (9) (2006) 1965–1974. doi:10.1364/JOSAB.23.001965.

[42] C. Caucheteur, Y. Shevchenko, L.-Y. Shao, M. Wuilpart, J. Albert, High resolution interrogation of tilted fiber grating SPR sensors from polarization properties measurement, Opt. Express 19 (2) (2011) 1656–1664. doi:10.1364/OE.19.001656.

[43] X. Chen, J. Xu, X. Zhang, T. Guo, B. Guan, Wide Range Refractive Index Measurement Using a Multi-Angle Tilted Fiber Bragg Grating, IEEE Photonics Technol. Lett. 29 (9) (2017) 719–722. doi:10.1109/LPT.2017.2682183.